processes

MDPI

Article

Biomass-Derived Activated Carbon as a Catalyst for the Effective Degradation of Rhodamine B dye

Shamim Ahmed Hira, Mohammad Yusuf, Dicky Annas, Hu Shi Hui and Kang Hyun Park *

Department of Chemistry, Pusan National University, Busan 46241, Korea; shamimsust44@gmail.com (S.A.H.); yusuf.chem.kor@gmail.com (M.Y.); annas.dickyy@gmail.com (D.A.); sheen_vi@163.com (H.S.H.)

* Correspondence: chemistry@pusan.ac.kr; Tel.: +8251-510-2238

Received: 19 June 2020; Accepted: 30 July 2020; Published: 2 August 2020

Abstract: Activated carbon (AC) was fabricated from carrot waste using $ZnCl_2$ as the activating agent and calcined at 700 °C for 2 h in a tube furnace. The as-synthesized AC was characterized using Fourier-transform infrared spectroscopy, X-ray diffraction analysis, scanning electron microscopy, transmission electron microscopy, X-ray photoelectron spectroscopy, and Brunauer–Emmett–Teller analysis; the results revealed that it exhibited a high specific surface area and high porosity. Moreover, this material displayed superior catalytic activity for the degradation of toxic Rhodamine B (RhB) dye. Rate constant for the degradation of RhB was ascertained at different experimental conditions. Lastly, we used the Arrhenius equation and determined that the activation energy for the decomposition of RhB using AC was approximately 35.9 kJ mol^{-1}, which was very low. Hopefully it will create a great platform for the degradation of other toxic dye in near future.

Keywords: Activated carbon; degradation; Rhodamine B; reaction rate; activation energy

1. Introduction

Water, crucial to sustain life on Earth, is predominantly polluted via the direct discharge of waste from various industries [1,2]. Wastewater from different industries, such as the paper, pharmaceutical, dyeing, chemical, petrochemical, and glass and ceramics ones, contains hazardous and intractable inorganic and organic pollutants that can damage the environment [3]. Dyes are common pollutants that are directly released into water bodies. Very commonly used dyes are Methyl Orange (MO), Methylene Blue (MB), Methyl Red (MR) and Rhodamine B (RhB) etc. RhB is an important dyestuff, which is easily soluble in water and is extensively used in various industries and laboratories [4,5]. It is a very toxic dye that contains four N-ethyl groups at both sides of a xanthene ring, which render it toxic and contribute to its carcinogenic and mutagenic properties [6]. Therefore, it is important to degrade RhB from wastewater for the sustainability of ecosystems.

Numerous RhB degradation techniques have been described in the literature, and the most common ones include photocatalytic [7–9] and sonochemical degradation [10], ultrasonic [11] and microbiological decomposition [12], and the adsorption of RhB on various organic and inorganic matrices. While most scientists have emphasized the importance of photocatalytic degradation, a few of them have also studied the conventional catalytic degradation process, which is a highly facile and reliable process compared to other techniques. To date, different noble metal-based catalysts, including Au-, Pt-, and Pd-based ones, have been used for the removal of dyes [13,14]. However, their high cost and low availability have limited their practical applications. Moreover, these catalysts require organic capping agents to prevent the aggregation of nanoparticles. Therefore, it is important to develop a low cost, readily available, and eco-friendly material for the effective degradation of dyes.

Activated carbon (AC) can be used efficiently to remove dyes because of its high surface area and porous structure [15]. Although AC is efficient for the catalytic degradation of RhB, its high cost is

a disadvantage. Therefore, low cost materials can be potential alternative precursors for fabricating AC. In the past, AC that has been obtained from palm [16] and coconut shells [17], rice husk [18], or jute sticks [19] has been used for the effective removal of RhB from aqueous solutions. Carrots are inexpensive vegetables which is very easy to collect. However, large amounts of carrots remain unused and are treated as waste. Thus, it was important to determine an effective way to use carrot waste. In addition to being inexpensive, carrot waste is nontoxic and non-hazardous and could be green processed without using any reducing agents. To the best of our knowledge, to date, no reports have been published on the use of carrot powder-derived AC for the removal of RhB from wastewater.

Here, we fabricated AC from carrot powder using $ZnCl_2$ as the activating agent. The as-fabricated AC exhibited a high surface area and porosity and was further used for the degradation of RhB dye. The carrot-derived AC further displayed good catalytic efficiency for the degradation of RhB in the absence of reducing agents. The effects of different parameters, such as the dye concentration, catalyst dosage, temperature, and pH, on the degradation process have been analyzed. Most catalytic degradation studies require extensive time to achieve effective degradation of the analyzed compounds [20,21]; however, the catalyst we fabricated required a short time to degrade RhB dye from aqueous solutions. Analyzing the kinetics of the degradation reaction is also important for that kind of study. The calculated activation energy for the catalytic degradation of RhB dye using the carrot-derived AC catalyst was 35.9 kJ mol^{-1}, which was much smaller than the values reported in some other studies. For example, Li et al. reported on rice-hull based silica supported iron catalyst for the efficient removal of RhB with the activation energy of about 82.35 kJ mol^{-1} [22]. In another study, Li et al. reported a Cu (II)-pyridyl complex on silica microspheres for the degradation of RhB at neutral pH with an activation energy of about 38.6 kJ mol^{-1} [23]. Furthermore, the reusability of the catalyst was also studied. We reused the fabricated AC for ten consecutive cycles without showing a significant decrease in its catalytic efficiency. Overall, the process of catalytic degradation was eco-friendly, green, and reliable, and we anticipate that similar materials could be used for the effective degradation of other toxic dyes in the future.

The schematic representation of the mechanistic study of RhB degradation is depicted in Scheme 1. Several functional groups were present on the surface of AC, and they can interact with the RhB dye molecules. The possible interactions could be described briefly as follows: (a) interactions between the –COOH groups of AC and electronegative moieties of RhB, (b) hydrogen bonding between the –OH groups of AC and aromatic ring of RhB, (c) hydrogen bonding between the –OH groups of AC and xanthene group of RhB, and (d) electrostatic interactions between the surface functional groups of AC and RhB dye molecules.

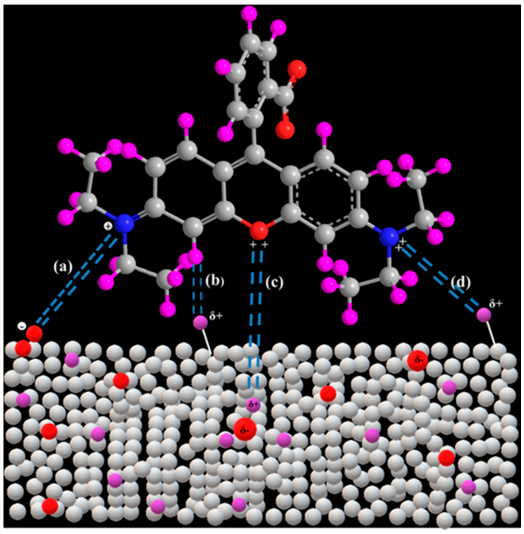

Scheme 1. Mechanism for the degradation of RhB on activated carbon.

2. Materials and Methods

2.1. Materials

Rotten carrots were obtained from a local market in Busan, South Korea. RhB, $ZnCl_2$ (99%), and HCl (37%) were purchased from Sigma Aldrich Chemical Co., Ltd. (St. Louis, MO, USA) and were used as-received without further purification. Deionized water was utilized throughout the study.

2.2. Fabrication of AC

AC was fabricated using a previously described method that we have slightly modified [24]. The collected carrots were properly washed, cut into small pieces, and dried in an oven at approximately 100 °C for 24 h. Afterward, the dried carrots were crushed into powder using a mortar and pestle. Next, the powder was mixed with $ZnCl_2$ at the mass ratio of 1:2. The resultant material was then heated in a tube furnace at 700 °C for 2 h followed by washing it three times with 10 mL of 10% HCl solution and 10 mL warm water until the pH of the filtrate was neutral. Subsequently, the obtained material was dehydrated under vacuum and the final product was denoted as AC-700 (Scheme 2). For comparison, two other samples were prepared by mixing $ZnCl_2$ and carrot powder at the same mass ratio indicated above. The resultant material was then heated in a tube furnace at 600 and 800 °C and the final products were denoted as AC-600 and AC-800, respectively.

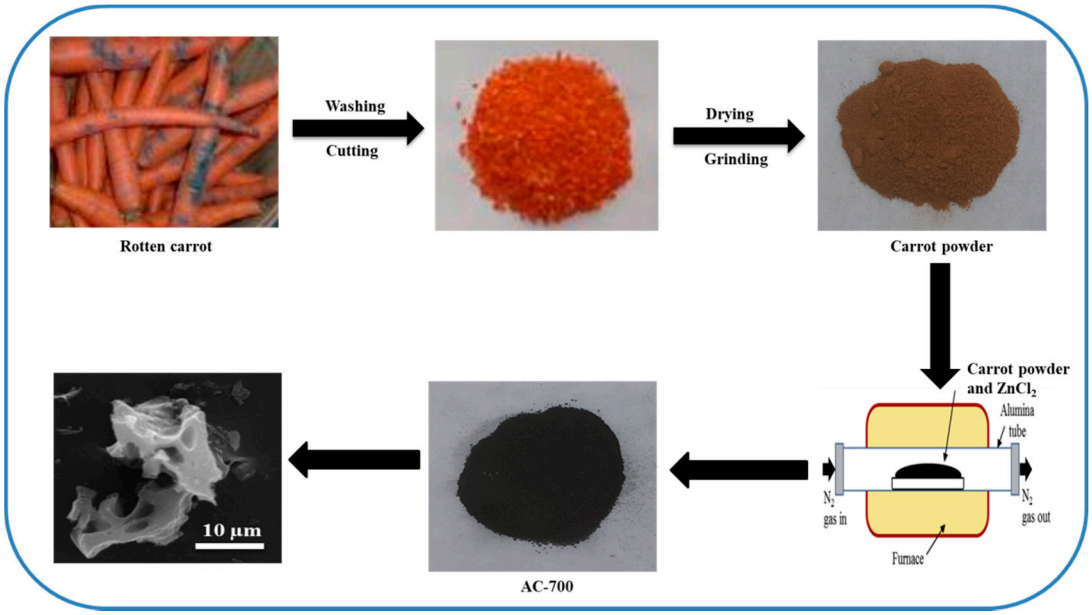

Scheme 2. The fabrication processes of activated carbon.

2.3. Characterization

A Nicolet 380 (Thermo Fisher, Waltham, MA, USA) Fourier transform infrared (FT-IR) spectroscopy instrument was utilized to investigate the chemical nature of the materials using KBr pellets. A RINT 2200 HK (Rigaku, Tokyo, Japan) X-ray diffraction (XRD) system was utilized for the structural analysis of the samples. A VEGA 3 (TESCAN, Tokyo, Japan) instrument was used to perform scanning electron microscopy (SEM) investigations. A SUPRA 40 (Zeiss, Oberkochen, Germany) spectrometer was used for energy-dispersive X-ray spectroscopy (EDS) analysis. A Talos F200X FEG (Thermo Fisher, Waltham, MA, USA) scanning transmission electron microscope (200 kV) was used for transmission electron microscopy (TEM) measurements. The Brunauer–Emmett–Teller (BET) surface area and total pore volume of the catalyst samples were determined using their N_2 sorption isotherms at 77 K using a BET ASAP 2020 (Micromeritics, Japan) surface area analyzer after the samples were degassed under N_2 flow

at 200 °C. X-ray photoelectron spectroscopy (XPS) profiles were obtained using a high-performance K-ALPHA+ (Thermo Scientific, Waltham, MA, USA) apparatus. Lastly, a UV-1800 (Shimadzu, Kyoto, Japan) spectrometer was used to analyze the catalytic degradation of dye. A tube furnace of Lindberg Blue M (TF55035C-1, Japan) was used for calcination purpose.

2.4. Catalytic Degradation and Kinetics Study

The catalytic efficiency of the fabricated AC carbon was examined for the RhB degradation. Firstly, 50 mL RhB solution (20 mg L^{-1}) was taken into a beaker, and then AC (0.3 g L^{-1}) was added to it under constant stirring. The degradation reaction was analyzed using ultraviolet–visible (UV–vis) absorption spectroscopy at constant time intervals (1 min) at the maximum wavelength, λ_{max}, of 554 nm, and the degradation efficiency was calculated using the following equation:

$$\text{degradation efficiency } (\%) = \frac{C_0 - C}{C_0} \times 100 = \frac{A_0 - A}{A_0} \times 100 \quad (1)$$

where C_0 and C are the concentration of RhB at time t = 0 and t = t where as A_0 and A are the absorbance of RhB at λ_{max} = 554 nm at time t = 0 and t = t respectively. The ratio of C to C_0 (C/C_0) was calculated from the ratio of the absorbance's A/A_0 at 554 nm.

The order with respect to RhB was carried out in the presence of AC. The order with respect to AC was determined in the presence of different excess amount of it while keeping other parameters as constant. After the addition of the dye, the absorbance of the solution was recorded every 1 min. The rate equation for the degradation of RhB can be expressed as,

$$\text{Rate} = \kappa_{app}[AC]^n[RhB]^m = \kappa_{app}\,[RhB]^m \text{ with } \kappa_{app}[AC]^n \quad (2)$$

where, κ_{app} is the apparent rate constant of the reaction, m and n are the pseudo order of the reaction with respect to RhB and AC respectively. The rate constant of the reaction was calculated from the slope.

3. Results and Discussion

3.1. Physico-Chemical Characterization of AC

SEM and TEM analyses were performed to analyze the morphology of the fabricated AC. The SEM and TEM images (Figure 1a–c), respectively illustrate the porous structure of the fabricated AC. It reveals that the $ZnCl_2$ was effective to create the porous structure. Similar findings were shown for the activated carbon obtained from different sources [25,26]. The map data (Figure 1d) confirms the presence of C and O atom and reveals that the O atoms were uniformly distributed throughout the carbon matrix of AC and no other impurities were present in the samples, which was further confirmed using EDS images (Figure S1). Figure 1e,f presents the elemental mappings of C and O atoms, respectively. The map data shows the uniform distribution of C and O throughout the matrix.

FT-IR characterization was conducted to identify the surface functional groups of AC. Figure S2 illustrates the FT-IR spectrum of AC. The pronounced band at 3400–3550 cm^{-1}, which was associated with the stretching mode of the –OH groups, has been commonly reported in the literature [27]. The peak at approximately 1550–1650 cm^{-1} was ascribed to the asymmetric stretching mode of the $–COO^-$ ions and the broad peak at 1000–1100 cm^{-1} were attributed to the presence of the C–O–C functional groups in the structure of AC. The small peak at approximately 500–600 cm^{-1}, which was associated with the C–H out-of-plane bending mode of the benzene derivative, has also been very commonly observed in the FT-IR spectra of AC samples [27].

XRD analysis was performed to elucidate the phase constitution of the fabricated AC, and the XRD patterns of the fabricated AC are depicted in (Figure S3). The degree of crystallinity of AC increased as its activating temperature increased. The two broad diffraction peaks at approximately 2θ of 24° and 43° in the XRD profile of AC were attributed to its (002) and (100) planes [28], and confirmed

the amorphous structure of the fabricated AC. Moreover, the XRD patterns of all AC samples were similar, which demonstrated that the calcination temperature did not significantly affect their structure. To determine the specific surface area and porosity of the fabricated material BET and porosity measurement was essential. The resultant nitrogen adsorption-desorption isotherms of AC prepared at different temperature has been displayed in (Figure 2). Nitrogen uptake increases with increasing the activation temperature from 600 °C to 700 °C. Further increase in temperature shows decrement of N_2 uptake capacity. Similar trends were obtained for activated carbon from peanut at different temperature [29]. The results regarding to BET surface area and total pore volume is summarized in Table 1. XPS analysis was necessary to investigate the surface chemical composition of the fabricated AC samples. The XPS survey spectrum of AC confirmed the presence of C and O in the samples (Figure S4). The high resolution C1s and O1s XPS profiles of AC are displayed in Figure 3. The C=C degenerate peak, which corresponded to the graphitic carbon linked to the main component, was observed at the binding energy of ~284.5 eV (Figure 3a). Other less intense degenerate peaks were observed at ~285.8, ~287.7, and ~290.8 eV, and corresponded to the C–O, C=O, and O–C=O functional groups, respectively. The deconvoluted peaks of O1s, which were observed at approximately 532.3 and 533.5 eV corresponded to the C–O and C=O functional groups, respectively (Figure 3b) [30,31]. These functional groups could play significant roles for the effective degradation of the RhB dye. The C (94.6%) and O (5.4%) content of the fabricated AC samples is listed in Table S1, and the values are in agreement with the EDS data (C (95.9%) and O (4.1%)).

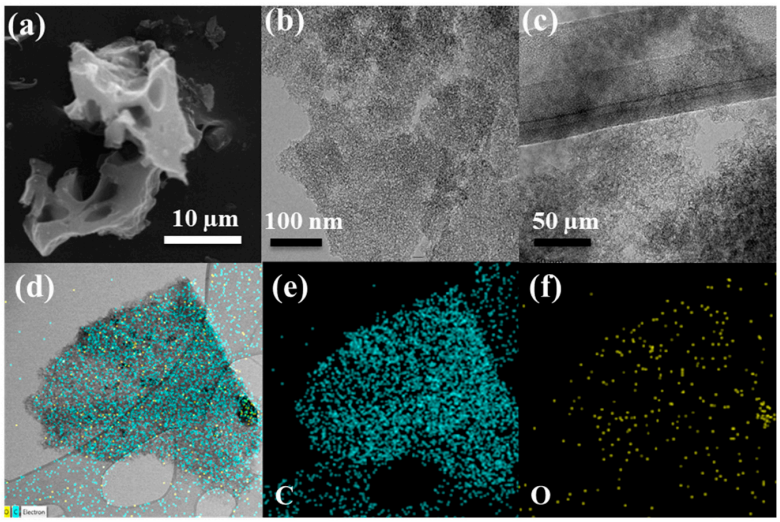

Figure 1. SEM image (**a**), TEM images (**b**,**c**), Map data (**d**) and elemental mapping (**e**,**f**) of AC-700.

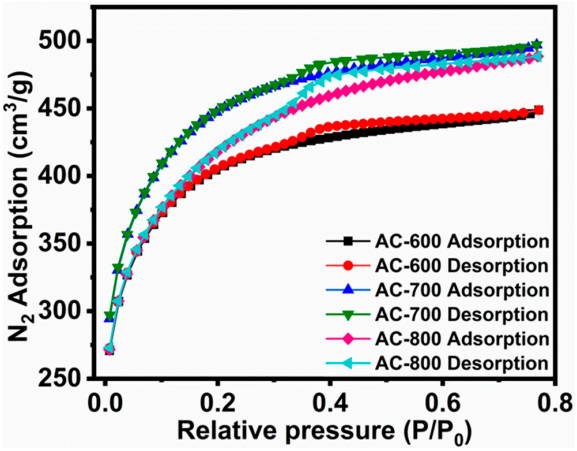

Figure 2. N_2 Adsorption-desorption isotherms of activated carbons.

Table 1. Pore structure characteristics of Activated carbon.

Sample	BET Surface Area (m^2/g)	Pore Size (nm)	BJH Adsorption Pore Volume (cm^3/g)
AC-600	1365.5	2.03	0.233
AC-700	1509.7	2.14	0.332
AC-800	1405.8	2.07	0.274

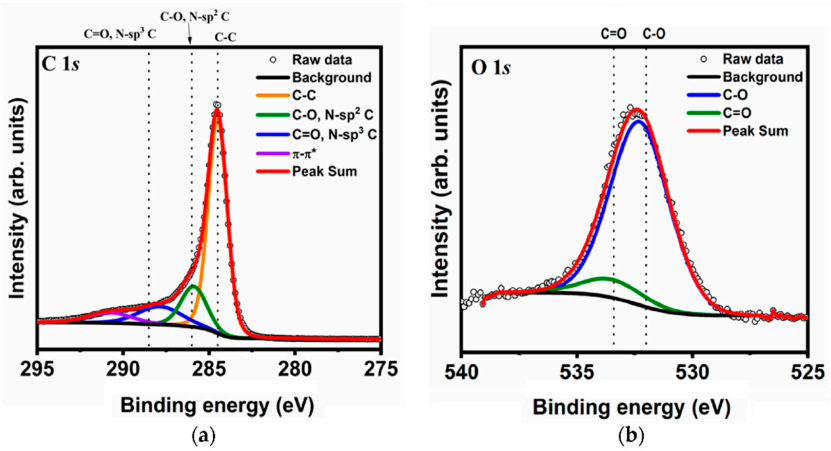

Figure 3. XPS patterns of AC-700 (**a**) C1s and (**b**) O1s.

3.2. Evaluation of Catalytic Activity of AC

During the degradation of RhB de-ethylation happens which results the production of leuco RhB (Scheme 3). We investigated the catalytic efficiency of the fabricated AC for the degradation of RhB, and also the effects of different experimental parameters, such as the catalyst type variation, initial dye concentration, catalyst dosage, pH, and temperature, on the degradation process.

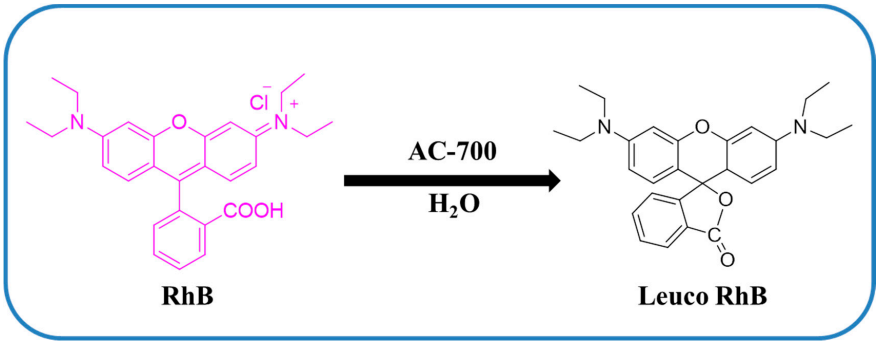

Scheme 3. Degradation mechanism of RhB.

3.2.1. Variation of Catalyst's Type

The activated carbon materials prepared at different temperature has been applied as catalyst for the effective dye degradation under same conditions. Figure S5 depicts the time dependent UV–vis absorption spectra for the catalytic degradation of RhB with different types of catalyst. The AC-700 catalyst can degrade the RhB quicker than AC-600 and AC-800. It's may be because of the high surface area of AC-700. Catalytic result with different types of catalysts has been summarized in Table S2.

3.2.2. Effect of pH

The pH of the solution is an important factor that affects the degradation rate. Degradation experiments were carried out in the wide pH range of 3–12 (Figure S6). Figure 4a displays the C/C_0 versus time curve for the degradation of RhB at different pH values. As the pH increased from 3 to 10 the degradation

of RhB also increased, and the highest degradation was observed at pH 10. When the pH was further increased, the degradation of RhB decreased. Therefore, pH 10 was selected to be the optimum pH for the subsequent experiments while keeping the other optimum condition as constant i.e., catalyst types AC-700, initial concentration of RhB (20 mg L^{-1}), catalyst dosage (0.3 g L^{-1}), and temperature (298 K). The surface of the catalyst becomes positive and negative charge in acidic and basic medium respectively. On the other hand, RhB is a basic dye that produces cation in water. So the catalyst repels this dye in the acidic medium. So less degradation occurs in acidic medium compared to basic medium. On the contrary, as in basic medium the catalyst is negatively charged, the adsorption becomes easier and that's why the degradation is increased. Several researchers have reported similar trends for the degradation of RhB [32,33]. The catalytic results at different pH values are summarized in Table S2.

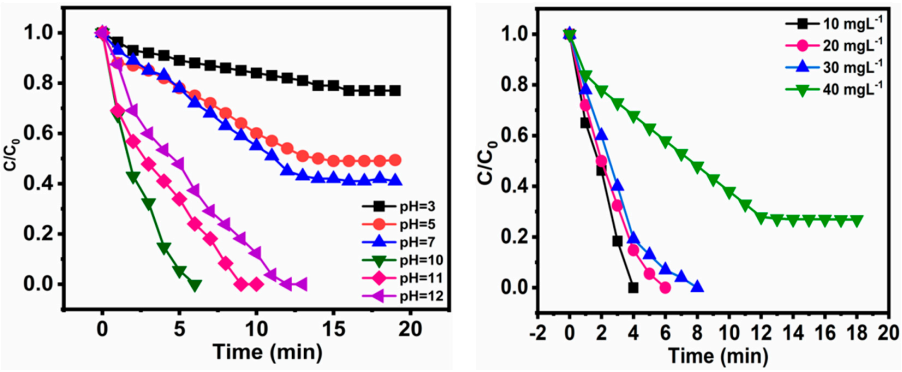

Figure 4. (**a**) C/C_0 versus time curve for the degradation of RhB with different concentration dye in the presence of AC-700 and (**b**) C/C_0 versus time curve for the degradation of RhB at different pH.

3.2.3. Initial Dye Concentration

The initial dye concentration is another critical factor for the degradation of RhB. Degradation experiments were performed by varying the initial RhB dye concentration between 10 and 40 mg L^{-1} (Figure S7). Figure 4b displays the C/C_0 versus time curve for the degradation of RhB at different initial RhB dye concentrations. As the initial RhB dye concentration increased, the time required for its complete degradation increased. However, for the initial RhB dye concentration of 40 mg L^{-1}, a degradation efficiency of approximately 87% was achieved after 2 h. If the initial RhB dye concentration increased beyond 40 mg L^{-1} the active sites of the catalyst were blocked and the degradation efficiency decreased. In addition, even the decolorizing was delayed at higher initial RhB concentrations [34]. Conversely, if the initial dye concentration is low the active sites could degrade the dye more easily. Furthermore, we determined that the rate constant for the degradation reaction which decreased as the initial RhB dye concentration increased (Table S2).

3.2.4. Effect of Catalyst Dosage

Catalyst dosage is another important parameter for the degradation process. The increase in catalyst dosage would increase the number of active sites on the catalyst surface, which would facilitate degradation. Figure S8 illustrates the time dependent UV–vis absorption spectra for the degradation of RhB at various catalyst loadings in the range of 0.1 to 0.4 g L^{-1}. At the AC loading of 0.1 g L^{-1} the degradation efficiency was only 23%. As the catalyst dosage increased, the degradation efficiency also increased, and the best degradation efficiency was achieved at the catalyst dosage of 0.3 g L^{-1}. Further increase in the catalyst dosage did not lead to an increase in the rate of degradation. Therefore, it could be inferred that as the catalyst dosage further increased, the active sites might overlap or agglomerate, which would hinder the degradation process. A similar trend was reported by Wang et al. [35]. Table S2 illustrates the changes in the degradation efficiency of the RhB dye by the catalyst as the catalyst dosage increased.

3.2.5. Effect of Temperature

Temperature significantly affected the degradation of RhB. We analyzed the degradation of RhB over the temperature range of (298–318 K) (Figure S9). As the temperature increased, the degradation rate also increased (Figure 5a). This can be explained using the collision theory. As the temperature increases, the number of collisions between molecules would increase, which would increase the degradation rate. The rate constant dependence on temperature is summarized in Table S2. The activation energy was calculated using the Arrhenius law and the lnk versus 1/T plot depicted in Figure 5b [36], as follows:

$$\ln k = \ln A - \frac{E_a}{RT} \quad (3)$$

where A is the pre-exponential factor, E_a is the activation energy (kJ mol^{-1}), R is the perfect gas constant (8.3 J·mol^{-1} K^{-1}) and T is the absolute temperature (K) and k is the reaction constant. The calculated E_a was approximately 35.9 kJ mol^{-1}, which was smaller than the values reported in the literature [23].

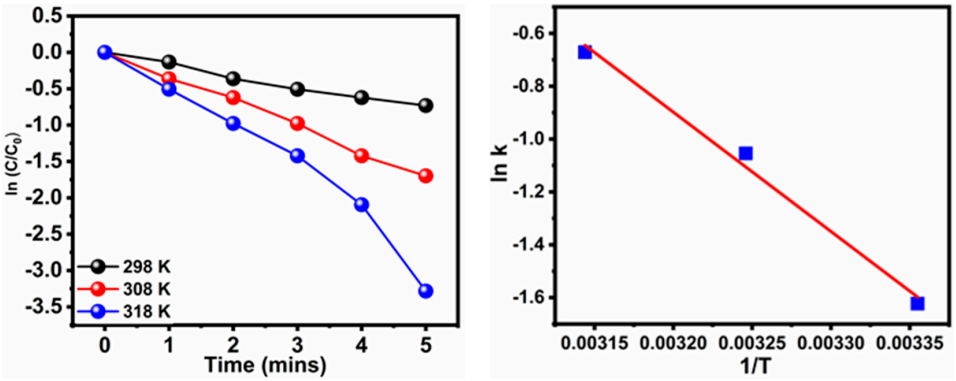

(**a**) (**b**)

Figure 5. (**a**) ln C/C_0 versus time curve for the degradation of RhB in the presence of AC-700 at different temperature and (**b**) Arrhenius plot (lnk versus 1/T curve).

4. Recyclability Study

Recyclability is very important to estimate the catalytic activity for practical applications. Recycling experiments were performed under the same experimental conditions. It was seen that our fabricated catalyst retained 85% of its initial catalytic activity after the 10th run. This was attributed to the loss of small amounts of catalyst during washing. The recyclability performance of the catalyst after the 10th cycle is displayed in Figure 6.

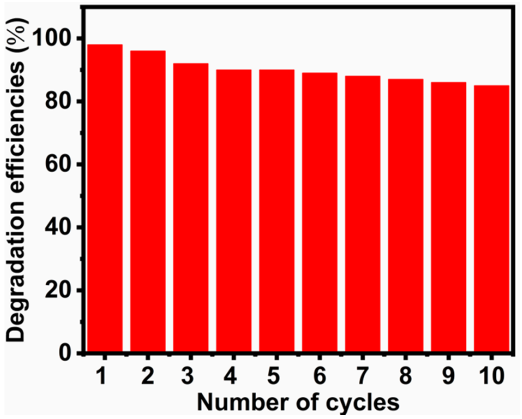

Figure 6. Recyclability study of the activated carbon until 10 consecutive cycles for the degradation of RhB.

5. Conclusions

In this study, we fabricated porous AC from carrot waste using $ZnCl_2$ as the activating agent. The fabricated material was characterized using well-defined physico-chemical techniques, and was subsequently used for the degradation of RhB in the absence of reducing agents. The degradation efficiency of RhB in the presence of AC as the catalyst reached 100% within short time. Moreover, the results of our kinetics study revealed that the activation energy of the catalytic degradation reaction was approximately 35.9 kJ mol^{-1}. Therefore, we anticipate that this cost-effective, eco-friendly materials will be used for the degradation of other toxic dyes in the future.

Supplementary Materials: The following are available online at http://www.mdpi.com/2227-9717/8/8/926/s1, Figure S1: EDS spectrum of AC-700, Figure S2: FTIR spectrum of AC-700, Figure S3: XRD patterns of the fabricated activated carbon, Figure S4: XPS survey spectrum of AC-700, Figure S5: Time dependent UV-vis absorption spectra for the degradation of RhB dye in the presence of different types of catalyst (a) AC-600 (b) AC-700 (c) AC-800, Figure S6: Time dependent UV-vis absorption spectra for the degradation of RhB dye in the presence of AC-700 at different pH (a) pH = 3 (b) pH = 5 (c) pH = 7 (d) pH = 10 (e) pH = 11 (f) pH = 12, Figure S7: Time dependent UV-vis absorption spectra for the degradation of RhB dye in the presence of AC-700 with different concentration of dye (a) 10 mg L^{-1} (b) 20 mg L^{-1} (c) 30 mg L^{-1} (d) 40 mg L^{-1}, Figure S8: Time dependent UV-vis absorption spectra for the degradation of RhB dye in the presence of AC-700 with different amount of catalyst (a) 0.1 g/L (b) 0.2 g/L (c) 0.3 g/L (d) 0.4 g/L, Figure S9: Time dependent UV-vis absorption spectra for the degradation of RhB dye in the presence of AC-700 at different temperature (a) 25 °C (b) 35 °C (c) 45 °C, Table S1: Elemental analysis from EDS and XPS, Table S2: Catalytic results for the degradation of Rhodamine B with different parameters.

Author Contributions: S.A.H. Worked in the Methodology, Formal analysis; Visualization, Investigation and Writing the original draft of the manuscript. M.Y. took part Formal analysis. D.A. performed Visualization. H.S.H. worked in Methodology and Formal analysis. K.H.P. took part in revising, editing and in supervision. All authors have read and agreed to the published version of the manuscript.

Funding: We are grateful to National Research Foundation of Korea (NRF), ICT & Future Planning project NRF-2017R1A4A1015533 and NRF-2017R1D1A1B03036303 for our project.

Acknowledgments: The authors would also like to acknowledge everyone who has provided helpful guidance and would also like to thank the anonymous reviewers for their useful comments.

Conflicts of Interest: The authors declare no conflict of interest.

References

1. Khatri, A.; Peerzada, M.H.; Mohsin, M.; White, M. A review on developments in dyeing cotton fabrics with reactive dyes for reducing effluent pollution. *J. Clean. Prod.* **2015**, *87*, 50–57. [CrossRef]
2. Richardson, S.D.; Kimura, S.Y. Water Analysis: Emerging Contaminants and Current Issues. *Anal. Chem.* **2016**, *88*, 546–582. [CrossRef] [PubMed]
3. Kim, K.; Ihm, S. Heterogeneous catalytic wet air oxidation of refractory organic pollutants in industrial wastewaters: A review. *J. Hazard. Mater.* **2011**, *186*, 16–34. [CrossRef] [PubMed]
4. Mittal, A.; Malviya, A.; Kaur, D.; Mittal, J.; Kurup, L. Studies on the adsorption kinetics and isotherms for the removal and recovery of Methyl Orange from wastewaters using waste materials. *J. Hazard. Mater.* **2007**, *148*, 229–240. [CrossRef]
5. Richardson, S.D.; Willson, C.S.; Rusch, K.A. Use of Rhodamine Water Tracer in the Marshland Upwelling System. *Ground Water* **2004**, *42*, 678–688. [CrossRef] [PubMed]
6. Merouani, S.; Hamdaoui, O.; Saoudi, F.; Chiha, M. Sonochemical degradation of Rhodamine B in aqueous phase: Effects of additives. *Chem. Eng. J.* **2010**, *158*, 550–557. [CrossRef]
7. Yuan, Q.; Liu, Y.; Li, L.; Li, Z.; Fang, C.; Duan, W.; Li, X.; Yan, C. Highly ordered mesoporous titania–zirconia photocatalyst for applications in degradation of rhodamine-B and hydrogen evolution. *Microporous Mesoporous Mater.* **2009**, *124*, 169–178. [CrossRef]
8. Li, Y.; Sun, S.; Ma, M.; Ouyang, Y.; Yan, Y. Kinetic study and model of the photocatalytic degradation of rhodamine B (RhB) by a TiO_2-coated activated carbon catalyst: Effects of initial RhB content, light intensity and TiO_2 content in the catalyst. *Chem. Eng. J.* **2008**, *142*, 147–155. [CrossRef]
9. He, Z.; Sun, C.; Yang, S.; Ding, Y.; He, H.; Wang, Z. Photocatalytic degradation of rhodamine B by Bi_2WO_6 with electron accepting agent under microwave irradiation: Mechanism and pathway. *J. Hazard. Mater.* **2009**, *162*, 1477–1486. [CrossRef]

10. Merouani, S.; Hamdaoui, O.; Saoudi, F.; Chiha, M.; Pétrier, C. Influence of bicarbonate and carbonate ions on sonochemical degradation of Rhodamine B in aqueous phase. *J. Hazard. Mater.* **2010**, *175*, 593–599. [CrossRef]
11. Mehrdad, M.; Hashemzadeh, M. Ultrasonic degradation of Rhodamine B in the presence of hydrogen peroxide and some metal oxide. *Ultrason. Sonochem.* **2010**, *17*, 168–172. [CrossRef] [PubMed]
12. Ju, D.J.; Byun, I.G.; Park, J.J.; Lee, C.H.; Ahn, G.H.; Park, T.J. Biosorption of a reactive dye (Rhodamine-B) from an aqueous solution using dried biomass of activated sludge. *Bioresource Technol.* **2008**, *99*, 7971–7975. [CrossRef] [PubMed]
13. Nigra, M.M.; Ha, J.; Katz, A. Identification of site requirements for 4-nitrophenol using gold nanoparticles catalyst. *Catal. Sci. Technol.* **2013**, *3*, 2976–2983. [CrossRef]
14. Junejo, Y.; Baykal, A. Ultrarapid catalytic reduction of some dyes by reusable novel erythromycin-derived silver nanoparticles. *Turk. J. Chem.* **2014**, *38*, 765–774. [CrossRef]
15. Parab, H.; Sudersanan, M.; Shenoy, N.; Pathare, T.; Vaze, B. Use of Agro-Industrial Wastes for Removal of Basic Dyes from Aqueous Solutions. *Clean Soil Air Water* **2009**, *37*, 963–969. [CrossRef]
16. Lacerda, V.S.; Sotelo, J.B.; Guimaraes, A.; Navarro, S.; Bascones, M.; Gracia, L.M.; Ramos, P.; Gil, J. Rhodamine B removal with activated carbons obtained from lignocellulose waste. *J. Environ. Manag.* **2015**, *155*, 67–76. [CrossRef]
17. Bello, O.S.; Adegoke, K.A.; Fagbenro, S.O.; Lameed, O.S. Functionalized coconut husks for rhodamine-B dye sequestration. *Appl. Water Sci.* **2019**, *9*, 189. [CrossRef]
18. Guo, Y.; Zhao, J.; Zhang, H.; Yang, S.; Qi, J.; Wang, Z.; Xu, H. Use of rice husk-based porous carbon for adsorption of Rhodamine B from aqueous solutions. *Dyes Pigments* **2005**, *66*, 123–128. [CrossRef]
19. Panda, G.C.; Das, S.K.; Guha, A.K. Jute stick powder as a potential biomass for the removal of congo red and Rhodamine B from their aqueous solution. *J. Hazard. Mater.* **2009**, *164*, 374–379. [CrossRef]
20. Kumar, T.K.M.P.; Kumar, S.K.A. Visible-light-induced degradation of rhodamine B by nanosized Ag_2S–ZnS loaded on cellulose. *Photochem. Photobiol. Sci.* **2019**, *18*, 148–154. [CrossRef]
21. Xiao, X.; Ma, X.; Liu, Z.; Li, W.; Yuan, H.; Ma, X.; Li, L. Degradation of rhodamine B in a novel bio-photoelectric reductive system composed of *Shewanella oneidensis* MR-1 and Ag_3PO_4. *Environ. Int.* **2019**, *126*, 560–567. [CrossRef] [PubMed]
22. Gan, P.P.; Li, S.F.Y. Efficient removal of Rhodamine B using a rice-hull based silica supported iron catalyst. *Chem. Eng. J.* **2013**, *229*, 351–363. [CrossRef]
23. Yuan, Y.; Zhang, C.; Wei, H.; Wang, Q.; Li, K. In situ synthesis an dimmobilization of a Cu(II)-pyridyl comples and silica microspheres as a novel Fenton-like catalyst for Rhodamine B degradation at near neutral pH. *RSC Adv.* **2017**, *7*, 22825–22835. [CrossRef]
24. Ahmed, S.; Ahmed, A.; Rafat, M. Supercapacitor performance of activated carbon derived from rotten carrot in aqueous, organic and ionic liquid based electrolytes. *J. Saudi Chem. Soc.* **2018**, *22*, 993–1002. [CrossRef]
25. Zhang, S.; Tao, L.; Jiang, M.; Gou, G.; Zhou, Z. Single-step synthesis of magnetic activated carbon from peanut shell. *Mater. Lett.* **2015**, *157*, 281–284. [CrossRef]
26. Jiang, X.; Guo, F.; Jia, X.; Liamg, S.; Peng, K.; Qian, L. Synthesis of biomass-based porous porous graphitic carbon combining chemical treatment and hydrothermal carbonization as promising electrode materials for super capacitors. *Ionics* **2020**, *26*, 3655–3668. [CrossRef]
27. Sumathi, S.; Bhatia, S.; Lee, K.T.; Mohamed, A.R. Selection of best impregnated palm shell activated carbon (PSAC) for simultaneous removal of SO_2 and NO_x. *J. Hazard. Mater.* **2010**, *176*, 1093–1096. [CrossRef]
28. Jain, A.; Tripathi, S.K. Nano-porous activated carbon from sugarcane waste for supercapacitor application. *J. Energy Storage* **2015**, *4*, 121–127. [CrossRef]
29. Arbind, K.; Hara, M.J. Preparation and characterization of high surface area activated carbon from fox nut (*Euryale ferox*) shell by chemical activation with H_3PO_4. *Results Phys.* **2016**, *6*, 651–658.
30. Rosenthal, D.; Ruta, M.; Schlogl, R.; Minsker, L. Combined XPS and TPD study of oxygen-functionalized carbon nanofibers grown on sintered metal fibers. *Carbon* **2010**, *48*, 1835–1843. [CrossRef]
31. Luo, Q.; Huang, L.; Gao, X.; Cheng, Y.; Yao, B.; Hu, Z.; Wan, Z.; Xiao, X.; Zhou, J. Activated carbon derived from melaleuca bark for outstanding high-rate supercapacitors. *Nanotechnology* **2015**, *26*, 304004. [CrossRef] [PubMed]
32. Saeed, M.; Ahmad, A.; Boddula, R.; Inamuddin, I.; Haq, A.U.; Azhar, A. Ag@Mn_xO_y: An effective catalyst for photo-degradation of rhodamine B dye. *Environ. Chem. Lett.* **2018**, *16*, 287–294. [CrossRef]

33. Saeed, M.; Muneer, M.; Mumtaz, N.; Siddique, M.; Akram, N.; Hamayun, M. Ag-Co_3O_4: Synthesis, characterization and evaluation of its photo-catalytic activity towards degradation of rhodamine B dye in aqueous medium. *Chin. J. Chem. Eng.* **2018**, *26*, 1264–1269. [CrossRef]
34. Bai, C.; Gong, W.; Feng, D.; Xian, M.; Zhou, Q.; Chen, S.; Zhou, Y. Natuarl graphite tailings as heterogenous fenton catalyst for the decolorization of Rhodamine B. *Chem. Eng. J.* **2012**, *197*, 306–313.
35. Wang, L.; Zhang, J.; Zhao, R.; Li, C.; Li, Y.; Zhang, C. Adsorption of basic dyes on activated carbon prepared from *Polygonum orientale* Linn: Equilibrium, kinetic and thermodynamic studies. *Desalination* **2010**, *254*, 68–74. [CrossRef]
36. Hites, R.A. Calculating the confidence and prediction limits of a rate constant at a given temperature from an arrhenious equation using excel. *J. Chem. Educ.* **2017**, *94*, 398–400. [CrossRef]